Packaging For A Drug Delivery Microelectromechanical System

by

Hong Linh Ho Duc

B.S./M.S. Materials Engineering
Drexel University, 2002

Submitted to the Department of Materials Science and Engineering
in Partial Fulfillment of the Requirements for the Degree of

Master of Science in Materials Science and Engineering

at the

Massachusetts Institute of Technology
February, 2005

ARCHIVES

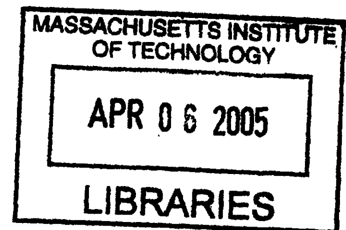

© Massachusetts Institute of Technology
All Rights Reserved

Signature of Author ....
Hong Linh Ho Duc
Dept. of Materials Science and Engineering
December 17, 2004

Certified by ....
Michael J. Cima
Sumitomo Electric Industries Professor of Engineering
Thesis Supervisor

Accepted by ....
Carl V. Thompson II
Stavros Salapatas Professor of Materials Science and Engineering
Chair, Departmental Committee on Graduate Students

Packaging For A Drug Delivery Microelectromechanical System

by

Hong Linh Ho Duc

Submitted to the Department of Materials Science and Engineering
on December 17, 2004, in Partial Fulfillment of the Requirements for the Degree of
Master of Science in Materials Science and Engineering

ABSTRACT

Local drug delivery is a fast expanding field, and has been a center of attention for researchers in medicine in the last decade. Its advantages over systemic drug delivery are clear in cancer therapy, with localized tumors. A silicon microelectromechanical drug delivery device was fabricated for the purpose of delivering chemotherapeutic agents such as carmustine, a potent brain cancer drug, directly to the site of the tumor.
Limitations in the delivery capacity of the device led to the design of a new package. This package is made from thermally bonded Pyrex® 7740 frames that are anodically bonded to the drug delivery chip. It increases the capacity of the chip, is smaller than the previous package and possesses true hermeticity, because of the bonding processes involved.
This work describes the fabrication steps of the new package and a problem with the thermal bonding of Pyrex® frames preventing the achievement of a package true to the original design. A temporary solution was devised and the completed package was tested with regards to its intended goals. It managed to increase the load capacity of the chip by a factor of 10, with potential for more, while decreasing the overall size of the package. Short-term hermeticity was achieved for this package by using a UV-cured epoxy to bond some pieces, which was not in the original design.
Future work will focus on finding a permanent solution to the aforementioned problem, and directions for it were suggested.

Thesis Supervisor: Michael J. Cima
Title: Sumitomo Electric Industries Professor of Engineering

ACKNOWLEDGEMENTS

My life at MIT is marvelous. I have all the means necessary to perform my research, conditions are ideal, I know everything I need to know, and the few problems that I've encountered were quickly solved... is what I'd like to say. Reality check. MIT is not marvelous. It is a hard-working place, where the problems that people encounter and sometimes spend a lifetime solving are what makes it a world-class institution. Luckily, while MIT is not marvelous, its people are. It is its people that enabled me to thrive and survive, and complete my thesis. I would like to offer my thanks to all those people, who made this thesis possible.

First, to my thesis supervisor, Michael Cima, for his insights and help, when I thought I was hopelessly stuck. His occasional prodding also helped me keep moving forward. He taught me that you can never rest on your laurels.

To the support staff of the CPRL, Barbara, Lenny and John, whose support made many an endeavor possible.

To my labmates in the Cima lab, Rebecca, Mindy, Grace and Karen, for their support and experience, and who taught me many useful things in my research, and in particular, Yawen, for teaching me almost everything I know about chip fabrication and packaging.

To the staff of the MTL, without whom no chip fabrication would ever have happened.

To the NIH, for their financial support of this project.

To my friends, who kept me grounded to reality, and reminded me that life exists out there...

To my parents, for bringing me up and making me who I am today.

Finally and most importantly, to my soon-to-be-wife, Nu, without whom life would just be a series of dreary moments. Her affection is what keeps me going day by day.

TABLE OF CONTENTS

LIST OF FIGURES 6

CHAPTER 1: DESIGN OF PACKAGE 8
1.1 Introduction 8
1.2 Issues with current package 11
1.2.1 Current design 11
1.2.2 Incomplete release 12
1.2.3 Leakage 14
1.2.4 Capacity 15
1.3 Package design 15
1.3.1 Parameters for improvement 15
1.3.2 Features of the new package 16
1.3.3 Material Selection 18
1.4 Thesis format 19
1.5 Acknowledgements 19

CHAPTER 2: MACHINING AND BONDING OF PYREX® 20
2.1 Machining of Pyrex® 7740 20
2.1.1 Design requirements 20
2.1.2 Glass machining techniques 20
2.1.2.1 Ultrasonic machining 21
2.1.2.2 Deep reactive ion etching 21
2.1.2.3 Hydrofluoric acid etching 21
2.1.2.4 Photosensitive glasses 22
2.1.2.5 Powder blasting 22
2.1.3 Experimental procedure 23
2.1.3.1 Powder blasting mask preparation 23
2.1.3.2 Powder blasting 24
2.1.3.3 Dicing 25
2.1.4 Results 26
2.1.5 Discussion 28
2.2 Thermal bonding of Pyrex® 7740 frames 29
2.2.1 Requirements for bonding 29
2.2.2 Experimental procedure 30
2.2.2.1 Cleaning 30
2.2.2.2 Thermal bonding 30
2.2.3 Results 31
2.2.4 Discussion 32

CHAPTER 3: ANODIC BONDING OF PYREX® TO SILICON CHIP 36
3.1 Introduction 36
3.2 Anodic bonding mechanism 36
3.3 Experimental procedure 39
3.3.1 Fixture 39
3.3.2 Anodic bonding procedure 40
3.4 Results 41
3.5 Discussion 42

CHAPTER 4: VALIDATION OF THE PACKAGE 44
4.1 Package completion 44
4.2 Experimental validation 45
4.2.1 Filling of devices 45
4.2.2 Hermeticity 46
4.2.3 *In vitro* release 47
4.3 Discussion 48

CHAPTER 5: CONCLUSION AND FUTURE WORK 51

REFERENCES 52

LIST OF FIGURES

Figure 1.1: Schematic of the silicon device and electrode configuration 10
Figure 1.2: Schematic of stainless steel package for drug delivery MEMS 11
Figure 1.3: Cumulative percentages of ^{14}C-BCNU released *in vitro* from two devices packaged using stainless steel frames and neoprene gasket 12
Figure 1.4: Optical micrograph of the cross-section of the stainless steel packaged device and detailed view of the gap between chip and gasket 13
Figure 1.5: Leak test of two stainless steel frame packaged devices sealed using neoprene gasket, with all outer edges of steel frames epoxied 14
Figure 1.6: Schematic of a type A frame overlayed over a silicon chip and schematic of the new package design 17

Figure 2.1: Pattern used to expose the photoresist film 24
Figure 2.2: Schematic of the powder blasting system used in machining the Pyrex® wafers 25
Figure 2.3: Top and cross-sectional views of a macroreservoir 27
Figure 2.4: Schematic of a pyramidal frustum and associated dimensions 28
Figure 2.5: Thermally bonded Pyrex® assembly and interface between macroreservoirs 31

Figure 3.1: Schematic of anodic bonding mechanism of Pyrex® 7740 and silicon 38
Figure 3.2: Picture of the anodic bonding fixture and experimental setup 40
Figure 3.3: Locations of successive probe placement for anodic bonding 41
Figure 3.4: Optical micrograph of hermetically bonded interface of a type A Pyrex® frame and silicon chip 42

Figure 4.1: Stainless steel package and Pyrex package for the drug delivery MEMS 45

Figure 4.2: Leakage test of a Pyrex® packaged device, compared to the stainless steel packaged devices from Figure 1.5 47
Figure 4.3: Cumulative percentages of ^{14}C-BCNU released from three Pyrex® packaged devices 48
Figure 4.4: Optical micrograph of the interface of a type A Pyrex® frame and a back plate bonded with UV-cured epoxy 49

CHAPTER 1: DESIGN OF PACKAGE

1.1 Introduction

Local drug delivery has received an enormous amount of focus from researchers in recent years, mainly because of the benefits that can be garnered from local delivery, as opposed to systemic delivery of drugs[1-12]. One such advantage is attained for carmustine. Carmustine (1,3-bis(2-chloroethyl)-1-nitrosourea, also called BCNU) is an effective brain cancer treatment drug, but its systemic toxicity level is too low for it to be injected intravenously at an efficient level. Local delivery through implantable devices has been shown to be more effective than systemic delivery, because it allows the drug concentration to be higher than toxic levels only in the region where the tumor resides, thereby avoiding generalized negative side effects. Implantable devices have been designed for delivery of such a drug. An example is Gliadel®, a polymer blend mixed with carmustine for continuous release of the drug[1, 2, 11].

Interleukin-2 is a cytokine which causes T-cell proliferation and elicits a natural killer response. It was also found to have an effect against tumors[13, 14]. Further investigations found that BCNU in combination with IL-2 could have a greater effect than either alone[7, 8, 15].

Our device is a silicon chip in which microreservoirs are etched and closed off with gold membranes which serve as addressable anodes, as shown schematically in Figure

1.1[10]. A large cathode is also patterned onto it. Drug in liquid or solid form is injected into the microreservoirs from the backside of the chip, which is then packaged.

The chip is implanted surgically. Gold is inert in the body, allowing the chip to conserve drugs inside the microreservoirs for long periods of time before activation. The activation consists of applying an anodic square wave potential to the gold membranes with respect to a blackened platinum reference (not shown), and using the large cathode as counter-electrode. The presence of chloride ions in body fluids in contact with the chip triggers the formation of gold chloride from the membranes upon application of the anodic potential. Gold chloride is soluble in water, resulting in the electrochemical dissolution of the gold anodes. This opens the microreservoirs and allows the drug to diffuse out of the device[9, 10, 16-21].

The features of our device are its lack of moving parts, and the possibility of controlled pulsatile release of different drugs, leading to a controlled release profile of multiple drugs in order to combine their effects. The drawback of such a device is the small size of its reservoirs, limiting the quantity of drug that can be released.

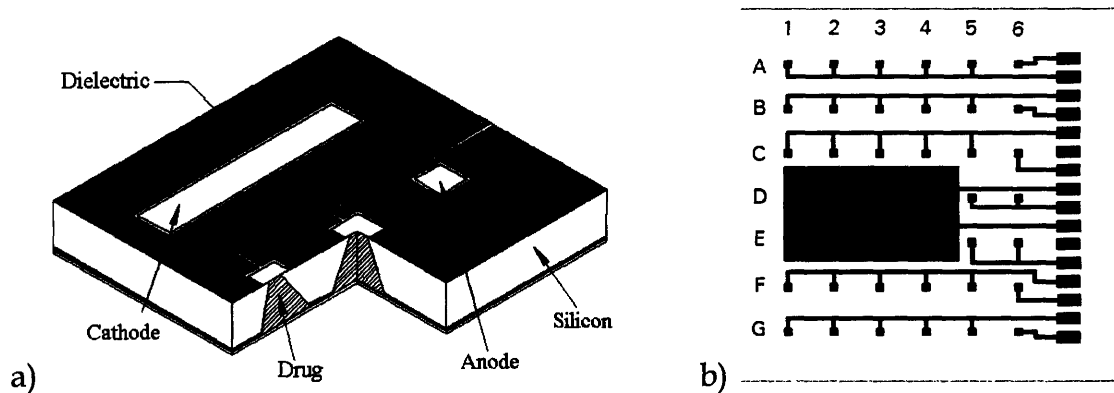

Figure 1.1: a) Schematic of the silicon device, showing microreservoirs covered by gold anodes, and the cathode nearby. The chip is protected by a dielectric layer, leaving only the gold anodes and cathode exposed. b) Electrode configuration of the silicon chip, showing individually addressable rows of anodes (A, B, C, F & G), as well as single anodes (Column 6) and double anodes (Rows D & E). Each anode seals off one microreservoir. Courtesy of Rebecca S. Shawgo.

1.2 Issues with current package

1.2.1 Current design

The current package consists of an assembly of stainless steel plates that are screwed together to form an enclosure for the silicon chip, schematically represented in Figure 1.2. A silicone or neoprene gasket covers the back of the chip to seal the microreservoirs and is pressed against the chip by a backing steel plate[19, 22]. The silicone gasket was replaced by neoprene for experiments involving BCNU when it was found that silicone was very permeable to BCNU. The combined volume of all accessible microreservoirs in the chip is 27 nL per reservoir x 34 (5 rows of 6 microreservoirs and 2 doublets) = 0.92 μL.

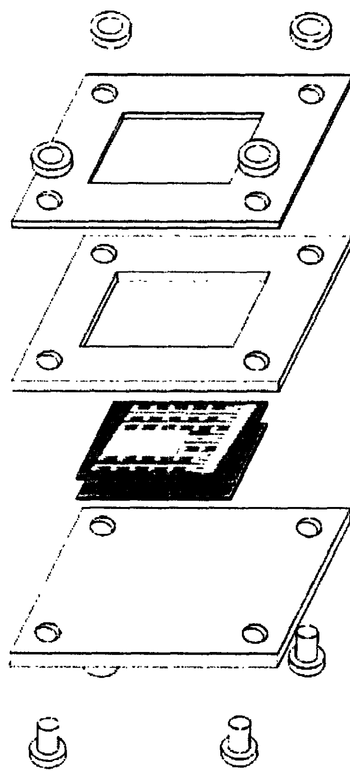

Figure 1.2: Schematic of stainless steel package for drug delivery MEMS. The top frame opening is smaller than the chip, to hold it in and allow front access to the chip. The middle frame surrounds the chip on all sides and the backing plate holds the gasket against the chip. The whole assembly is held together by nuts and bolts at the four corners. Not to scale. Courtesy of Rebecca S. Shawgo.

1.2.2 Incomplete release

This package was used for the release of BCNU *in vitro* and *in vivo*[16, 17, 19]. *In vitro* releases shown in Figure 1.3 revealed that not all of the drug injected in the microreservoirs was released. It was found that only 40% of the injected drug was released out of the chip. Scintillation counting of ^{14}C-radiolabeled BCNU for different parts of the disassembled package after activation revealed that 45% of the remaining radioactivity was found coming from the neoprene gasket, after soaking it for 3 days. The rest came from the epoxy and steel frames[16, 17].

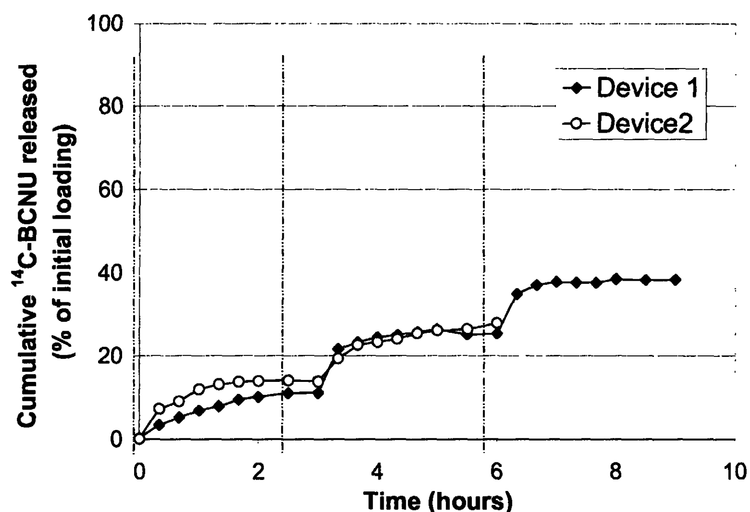

Figure 1.3: Cumulative percentages of ^{14}C-BCNU released *in vitro* from two devices packaged using stainless steel frames and neoprene gasket. Each activation (denoted by the dashed line) corresponds to opening of one row of reservoirs with 0.01 μCi loading. Each filled reservoir also contained 22 nL polyethylene glycol (PEG). Test performed at room temperature in PBS. Courtesy of Yawen Li.

Figure 1.4 shows a cross-section of a packaged chip. The chip was packaged, mounted in epoxy by vacuum infiltration, cross-sectioned and polished. Figure 1.4(b) shows a small gap between the gasket and the edge of the microreservoirs.

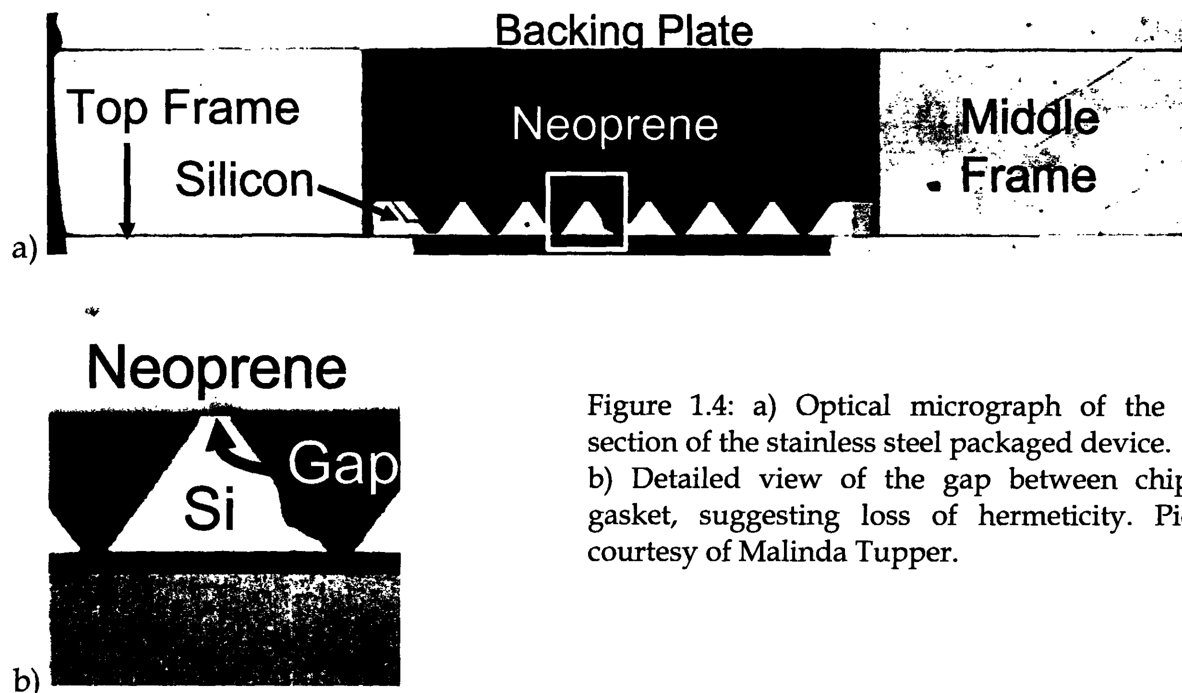

Figure 1.4: a) Optical micrograph of the cross-section of the stainless steel packaged device.
b) Detailed view of the gap between chip and gasket, suggesting loss of hermeticity. Pictures courtesy of Malinda Tupper.

The above observations suggest two important reasons why the release of drugs from the current package is incomplete. Firstly, the radioactivity measurements suggest that some of the drug partitioned into the neoprene. Neoprene is a rubbery material, containing free space in which the small BCNU molecule may partition. Secondly, the presence of radioactivity on the steel frames and the gap shown in Figure 1.4(b) indicate that the microreservoirs are not actually hermetically sealed. The liquid drug could then

wet the space between the chip and the gasket, and could travel all the way to the edge of the chip onto the stainless steel frames.

Only one drug was used in release experiments up to date, so the issue might not have been critical if released amounts were efficacious, but for future experiments involving more than one drug, achieving internal, i.e., reservoir-to-reservoir, hermeticity, is critical to keeping the drugs from interacting with each other before activation.

1.2.3 Leakage

Figure 1.5 shows a leakage test performed previously[17] with stainless steel packages. Epoxy was applied to the outer edges of the packages, but not their inside edges, where the top frame comes in contact with the chip. This test shows that the stainless steel package can leak out BCNU if epoxy is not applied on all of the edges of the package, including the inside edge of the top frame. As much as 20% of the loaded drug could escape in that case, starting almost immediately.

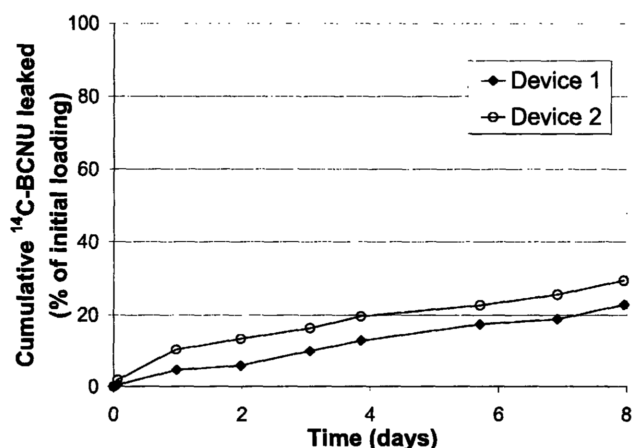

Figure 1.5: Leak test of two stainless steel frame packaged devices sealed using neoprene gasket, with all outer edges of steel frames epoxied. The ^{14}C-BCNU for both devices was 0.022 μCi. Each filled reservoir also contained 22 nL PEG. Test performed at room temperature in deionized water. Courtesy of Yawen Li.

1.2.4 Capacity

It was found in dose ranging experiments (not published) that at least 1.24 mg of carmustine was needed to significantly impede the growth of a tumor in rats. This corresponds to a volume of 1.24 µL, assuming a density of 1 mg/µL. BCNU also needs to be injected along with polyethylene glycol (PEG) to improve its release kinetics, studied elsewhere[17].

Interleukin-2 is in the same case. Chiron Proleukin® is the source of IL-2 being used, and contains a mixture of mannitol and sodium dodecyl sulfate buffered with sodium phosphate, added to the IL-2. The target load for delivery of IL-2 is 190 µg of Proleukin®. The corresponding volume is 3.6 µL of solution, when reconstituted with sterile water per manufacturer instructions.

The capacity of the chip (currently 0.9 µL) then becomes a major issue for the efficacy of the chip in treating tumors, compounded by the incomplete release demonstrated above.

1.3 Package design

1.3.1 Parameters for improvement

The previous sections demonstrated the need for a higher loading capacity in the chip, as well as problems with internal hermeticity of the chip. One possibility to overcome this lack of capacity is to use more than one chip at the same location. The size of the

current package (11 x 11 x 2.5 mm^3) precludes this possibility, however. This reasoning led to the need for designing a new package for the chip. The primary parameters considered were as follows:

- Increased drug load capacity of the chip
- Complete release of the loaded drug
- Internal hermeticity
- Environmental hermeticity (leakage to the outside of the package)

1.3.2 Features of the new package

The consideration of these parameters led to the design schematically represented in Figure 1.6. Figure 1.6(a) shows a 7.5 mm x 5.5 mm frame, which we will call type A frame. It is patterned and presents 2 rectangular through-holes 3020 μm long and 1080 μm wide, separated by 1320 μm. We will call these through-holes macroreservoirs from this point on. The given dimensions are such that these macroreservoirs are connected to 10 microreservoirs each on either side of the cathode on the chip, as shown with the underlying drawing of the back of a chip (see also Figure 1.1(b) for cathode location). The area under the cathode itself (in the middle of the chip) is sealed off between the two macroreservoirs. Frames with similar design can be stacked at will to increase the capacity of the macroreservoirs. Two of those frames have to have machined access channels leading to the macroreservoirs, for the drug to be loaded into them, as shown in Figure 1.6(b). They will be called type B frames. An unpatterned back plate is finally stacked at the top to close off the macroreservoirs.

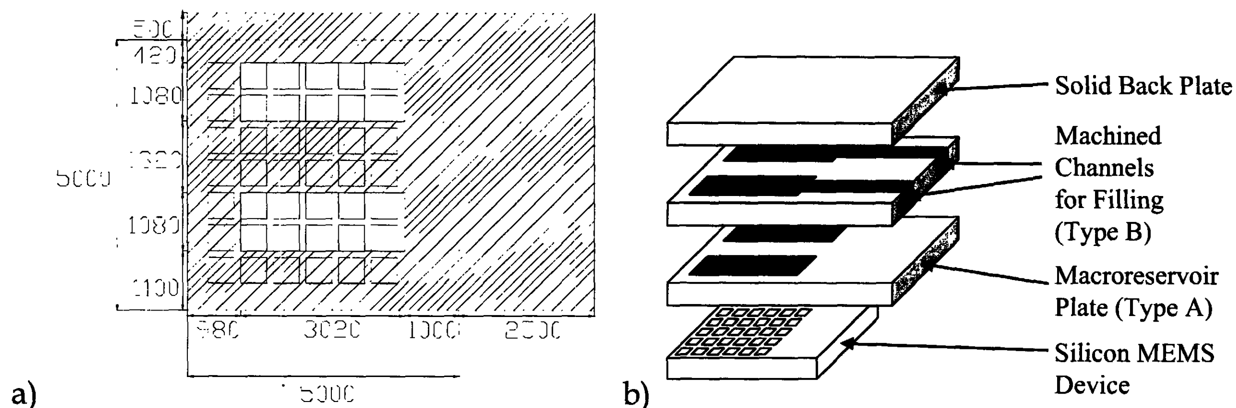

Figure 1.6: a) Schematic of a type A frame overlayed over a silicon chip, showing the alignment of macroreservoirs with 10 microreservoirs beneath them. Dimensions are in microns. b) Schematic of the new package design, showing one package frame of each type (not to scale). The actual package usually contains two type B frames and one type A frame, but any number of them can be stacked to extend the capacity of the macroreservoirs.

This arrangement allows increasing the capacity of the drug delivery chip at the expense of the ability to have separate loads in each microreservoir, as there are now 2 major reservoirs each connected to 10 microreservoirs. There is therefore less control over the delivery profile, since only 2 separate loads can be controlled. There can however be potentially some control over the rate of release if the number of open membranes is varied. Further experimentation will have to confirm that, however. It is also possible to pattern the frames differently such that more and smaller macroreservoirs are created, but this design is satisfactory for the current release requirements.

This design presents no mechanical means of attachment such as bolts and nuts. It is difficult to ensure hermeticity of packages with mechanical means of sealing without O-

rings. Implementing the use of O-rings on such a small chip is impossible without losing the use of many microreservoirs. The frames will instead be thermally bonded to each other, since such a bond would be strong and definitely hermetic. The critical decision is in finding a material that can achieve the same kind of bonding with the silicon chip, for total hermeticity.

1.3.3 Material Selection

The choice of a material for the package was made relatively obvious by the restrictions imposed by the materials present on the chip. The gold membranes covering the microreservoirs cannot be exposed to temperatures higher than 350°C. They would develop defects (voids, through-thickness grain boundaries) and compromise the hermeticity of the chip[17]. Thermal bonding of silicon would have to be done at higher temperatures to be reliable, and is thus not acceptable.

Anodic bonding is a technique that is gaining in popularity to bond glasses to silicon. It can be done at lower temperatures than thermal bonding, and can only be done with certain types of glass, because of the processes involved in the bonding. The mechanism of anodic bonding will be discussed in more depth in the following chapters. Pyrex® 7740 is the most widely used glass for anodic bonding to silicon and is therefore the material of choice. This is due to its thermal coefficient of expansion (3.25×10^{-6} °C^{-1}), which is close to that of silicon (2.6×10^{-6} °C^{-1}). The transparency of the glass to visible light is also useful for aligning the frame to the chip during bonding. The disadvantage of Pyrex® 7740 is that, like all glasses, its brittleness makes it difficult to machine.

1.4 Thesis format

Chapter 2 will cover the machining of the Pyrex® frames and subsequent thermal bonding into an assembly. A problem with the thermal bonding of the assembly will make Chapter 3 devoted to the anodic bonding of the chip, not to the previously made assembly, but to a single machined Pyrex® frame. Chapter 4 will present a solution to the aforementioned problem. It will also report on a leakage test and *in vitro* release of BCNU that highlight the performance of the new package with respect to the improvement parameters set forth in Section 1.3.1.

1.5 Acknowledgements

The fabrication of the silicon chips and anodic bonding procedure were performed in the Microsystem Technology Laboratories of the Massachusetts Institute of Technology. The author would like to acknowledge the help of the staff of the laboratory.

Acknowledgements go to Dr. Takamichi Ogawa, who performed the initial experiments in powder blasting in our group, and to Dr. Malinda Tupper, who created the procedure for bonding Pyrex® frames by UV-cured epoxy.

Drs. Yawen Li, Rebecca S. Shawgo and Malinda Tupper are also acknowledged for their permission to use some of their original material.

CHAPTER 2: MACHINING AND BONDING OF PYREX®

2.1 Machining of Pyrex® 7740

2.1.1 Design requirements

The package design requires macroreservoirs 3020 µm x 1080 µm to be etched through 500 µm-thick Pyrex® 7740 wafers. Dimensional and spatial tolerance can be no more than 50 µm, because the width of silicon between reservoirs on the back of the chip, where bonding is to occur, is 120 µm. After dicing the frames, some of them also need to have channels machined to access the macroreservoirs (type B frames).

2.1.2 Glass machining techniques

Glass is not easily machined because of its brittleness. One only has to see the bevy of different techniques used to machine it to recognize the difficulty of the issue. The most prominent ones are:

- Ultrasonic machining
- Deep reactive ion etching (RIE)
- Hydrofluoric acid (HF) etching
- Photosensitive glasses
- Powder blasting

2.1.2.1 Ultrasonic machining

Ultrasonic machining[23] (also called ultrasonic impact grinding) uses a tool that is vibrating in its longitudinal direction (perpendicular to the surface to be machined) at high frequencies (usually ≥ 20 kHz) and with a small amplitude (5-50 μm). A static load is applied to the tool and a slurry of abrasive particles is pumped to the machining zone. The vibration of the tool tips causes the abrasive particles in the slurry to impact the glass surface, removing material by microchipping. It is a reliable but expensive technique, because of the cost of tooling, which must be custom made to the desired pattern and replaced regularly from wear.

2.1.2.2 Deep reactive ion etching

Deep reactive ion etching (DRIE) is a standard technique used in MEMS fabrication, but usually for silicon. It uses sulfur hexafluoride (SF_6) plasma to etch Pyrex® wafers[24-26]. The desired pattern is transferred using a nickel mask. It has very good resolution (down to less than 1 μm), is very anisotropic, but is limited by slow etch rates (typically 0.60 μm/min).

2.1.2.3 Hydrofluoric acid etching

Hydrofluoric acid (HF) etching is an isotropic wet chemical process using diluted HF to dissolve glass protected by a metallic mask, [3, 27, 28]. The mask is patterned by standard photolithography techniques. Mask undercutting as well as pitting due to defects in the mask are common problems associated with this method[27]. Due to the

depth required for etching and mask undercutting issues, HF etching was not deemed ideal in this case.

2.1.2.4 Photosensitive glasses

Photosensitive glasses are glasses that can be patterned directly by photolithographic exposure, followed by curing and etching[29]. Commercially available photosensitive glasses are however unsuitable for anodic bonding to silicon because of their low thermal expansion coefficient.

2.1.2.5 Powder blasting

Powder blasting is the same as sandblasting, but with abrasive particles with a typical size range from 10 to 150 µm. It has gained acceptance in the MEMS community as a viable glass machining process[30-33], from its humble origins in glass decoration. It is also widely used in the fabrication of large plasma displays[34-37].

It is in essence an accelerated erosion process. An air jet projects abrasive particles against the glass, eroding it as many particles hit the surface of the glass. The actual mechanism is believed to be as follows[38, 39]: when a single particle hits the surface of the glass with enough velocity, it has been observed that cracks radiate from the point of impact, some of them connected by sub-surface lateral cracks. Subsequent impacts remove the chips thus formed, and introduce additional cracks, allowing the erosion to continue. The surface is patterned by a protective mask that leaves the areas to be etched bare. The mask can be organic or metallic[33, 40]. Powder blasting is anisotropic,

has a fast etching rate (~ 7 μm/s, dependent on abrasive media) and is inexpensive. It was therefore chosen as the method to etch the Pyrex® wafers.

2.1.3 Experimental procedure

2.1.3.1 Powder blasting mask preparation

Previous experimentation (not published) determined that a commercial polymeric mask used for art, UltraPro™ Self Adhesive Photoresist Film (PhotoBrasive Systems, Duluth, MN) was suitable as a mask for powder blasting to etch 480 μm squares through a 500-μm thick Pyrex 7740 wafer. The film is 125 μm thick and was patterned using a mask aligner (MJB3, SUSS Microtec, Waterbury Center, VT) with a 200W high-pressure mercury lamp and conventional chrome photomask carrying the pattern for type A frames (see Figure 2.1). The exposure time was 25 seconds. The UV cured film was then developed using a WaterPik WP72-W water jet system (Water Pik Technologies, Inc, Newport Beach, CA) to wash out non-exposed parts and dried at 37°C for 25 minutes.

The dried film was laminated onto a polished 500-μm Pyrex® 7740 wafer, 100 mm in diameter. Another polymeric mask was applied to the other side of the wafer, UltraPro™ Blue Self Adhesive Photoresist Film, from the same company. This 150-μm thick film underwent the same processing, except that the exposure time was 30 seconds and drying time was 30 minutes. It is formulated to be adjustable before lamination, so that it can be aligned with the previously applied film on the other side

of the wafer. Alignment was done optically under a stereoscope, such that the patterns would match exactly with each other, for 2-sided powder blasting.

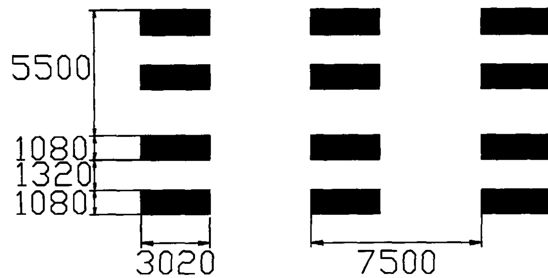

Figure 2.1: Pattern used to expose the photoresist films; black is chrome, i.e., regions in black will be etched. Dimensions and spacing of the rectangles, in micrometers, match the dimensions shown in Figure 1.6(a).

2.1.3.2 Powder blasting

Powder blasting was done in the Micro Jet 200 sandblasting system from Hunter Products, Inc. (Bridgewater, NJ). A schematic of the system is shown in Figure 2.2 (Courtesy of Takamichi Ogawa). Abrasive powder is mixed with a dry air stream and carried from the powder container to the glove box through a nylon tube into the nozzle. The nozzle is made of tungsten carbide for wear resistance and has an internal diameter of 0.76 mm.

The applied blasting pressure was 0.50 MPa, and the distance between the nozzle and the wafer was held to ~ 10 cm. The abrasive powder used was sharp aluminum oxide particles, with abrasive size #320 (Hunter Products, Inc., Bridgewater, NJ). The abrasive jet was moved in a zigzag pattern across the wafer in order to etch the wafer evenly, first on one side then on the other side, alternating between sides until the wafer was etched through. The polymeric mask was peeled off after rinsing in water.

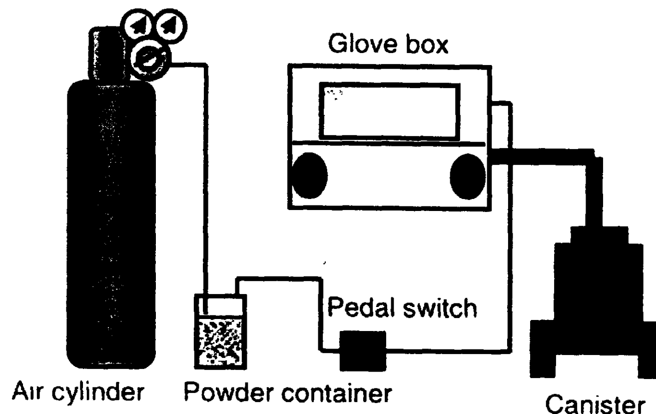

Figure 2.2: Schematic of the powder blasting system used in machining the Pyrex® wafers. The air cylinder sends compressed air through the powder container, carrying powder with it through the nylon tubing to the nozzle inside the glove box. An on-off pedal switch controls the flow of air. The canister is a vacuum cleaner which sucks in the powder in the glove box. It ensures a negative pressure in the glove box with respect to atmospheric pressure to avoid escape of powder. Schematic courtesy of Takamichi Ogawa.

2.1.3.3 Dicing

Wafers were diced into 5.5 mm x 7.5 mm frames in a diesaw (DAD 2H/6T, Disco Corporation, Tokyo, Japan) using a glass coated blade. Spatial alignment of the cuts with respect to the macroreservoirs location was done in the diesaw, using a built-in microscope and distance measuring routine. Type B frames were produced by encasing finished type A frames in mounting wax (MWM070, South Bay Technology, Inc, San Clemente, CA) between two microscope slides for mechanical support. Access channels were diced in an Isomet™ Low Speed Saw (Buehler, Ltd, Lake Bluff, IL) with a diamond coated blade. The frames were then immersed in chloroform overnight to dissolve the mounting wax and were further cleaned by sonication in soapy water and DI water.

2.1.4 Results

Figure 2.3 shows the top view and cross-section of a macroreservoir in an optical microscope. The inner red line in Figure 2.3(a) represents the original dimensions of the mask. The area between the two red lines represents the area of silicon available for anodic bonding of the silicon chip to the Pyrex® frame around the macroreservoir. If a defect crosses the outer red line, the macroreservoir will most likely have a leak to one of the surrounding microreservoirs. It can be seen that it is not the case in Figure 2.3(a). Figure 2.3(b) shows a cross-section of a macroreservoir. The cross-section was prepared by dicing across a macroreservoir with the diesaw mentioned in the previous section. The measured sidewall angle θ was ~ 67° on both sides of the wafer.

The volume of this macroreservoir is calculated by approximating its shape as two equal pyramidal frusta, although variations in processing may not make it so, as well as rounded corners. It is however a reasonable approximation.

The volume of a pyramidal frustum is calculated by:

$$V = \frac{h}{3}\left(A_1 + A_2 + \sqrt{A_1 A_2}\right) \qquad (1)$$

where the pertinent dimensions are given in Figure 2.4.

The volume of one frustum is then calculated as follows:

$$h = 0.25 \text{ mm}$$

$$A_1 = 3.02 \text{ mm} * 1.08 \text{ mm} = 3.26 \text{ mm}^2$$

$$x = h / \tan\theta = 0.25 \text{ mm} / \tan 67° = 0.106 \text{ mm}$$

$$A_2 = (3.02 \text{ mm} - 2\,x) * (1.08 \text{ mm} - 2\,x) = 2.44 \text{ mm}^2$$

$$V = \frac{h}{3}\left(A_1 + A_2 + \sqrt{A_1 A_2}\right) = \frac{0.25}{3}\left(3.26 + 2.44 + \sqrt{3.26 \times 2.44}\right) = 0.71\,\mu\text{L}$$

The total nominal volume of one macroreservoir is therefore double this number, 1.4 µL, and the capacity of one type A frame is **2.8 µL**. The capacity of a type A frame blasted from one side only turns out to be 2.4 µL. The actual macroreservoir volume should thus be somewhere between 2.4 and 2.8 µL. We use 2.8 µL as the maximum capacity of the frame.

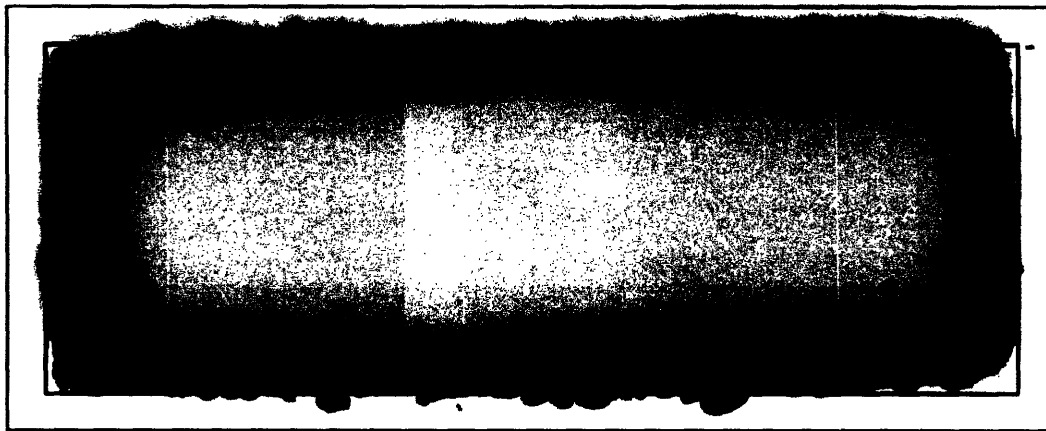

a)

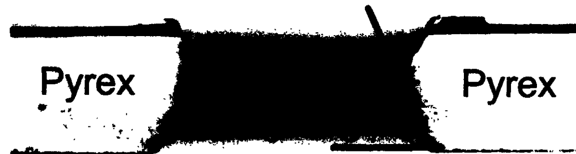

b)

Figure 2.3: a) Top view of a macroreservoir in a microscope. The inner red line represents the original dimensions of the mask. The outer red line is the limit for defect size at the edges, as larger defects would compromise the hermeticity of the macroreservoir. The black area is the sidewalls resulting from the powder blasting. b) Cross-sectional view of a macroreservoir. The measured sidewall angle θ was 67°.

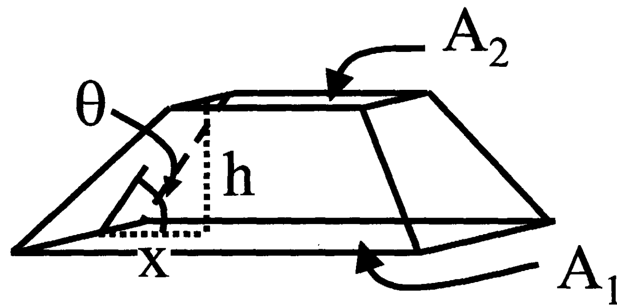

Figure 2.4: Schematic of a pyramidal frustum and associated dimensions.

2.1.5 Discussion

Experiments where the wafer was etched only on one side showed that the mask was eroded away as the blasting proceeded, resulting in overetching of the side walls (not published). Chipping on the far side of the wafer (with sizes greater than the tolerance limit) also occurred upon reaching through the wafer, which can be explained by impacting particles breaking off large chips from the far surface as the remaining thickness of the wafer is small. The reasons for using 2-sided blasting were thus:

- to avoid mask erosion by cutting exposure time of one side to the powder blasting process by half;
- to avoid chipping at the surface of the wafer by having the last amount of material removed in the bulk of the wafer, rather than at the surface. Impacting particles then cannot harm the surface when breaking off this last layer of material.

It can be seen in Figure 2.3 that the decision to use 2-sided blasting bore its fruits, as dimensional tolerances are met for the subsequent anodic bonding process.

2.2 Thermal bonding of Pyrex® 7740 frames

2.2.1 Requirements for bonding

The annealing point of a glass is the temperature at which internal stresses will be substantially relieved in 15 minutes ($\eta = 10^{13.2}$ Poise). The softening point of a glass is the temperature at which it will deform under its own weight ($\eta = 10^{7.6}$ Poise). Bonding of the Pyrex frames would have to happen between those two points, since at least some diffusion is needed for bonding to occur, but not so much that the frames would lose their shape. The other conditions for diffusion bonding are low surface roughness (< 15 Å) and a clean surface devoid of contamination, for intimate contact to happen between the frames. This intimate contact then allows the glass pieces to bond directly to each other.

The annealing point of Pyrex 7740 is 560°C and its softening point is 820°C, according to Corning specifications[41]. With clean surfaces and low surface roughness, two Pyrex® 7740 wafers can be completely bonded at 600°C for 30 minutes, without any additional compression loads needed[42].

2.2.2 Experimental procedure

2.2.2.1 Cleaning

The surface of the Pyrex frames to be bonded has to be absolutely clean in order for intimate contact and diffusion bonding to occur. The ideal case would be to clean the surfaces to be bonded with an oxygen plasma and do the bonding in a cleanroom. We were lacking this possibility and therefore had to find another cleaning method suitable enough for bonding.

Pieces to be bonded were first sonicated in soapy water. The next cleaning step used the Waterpik WP72-W water jet system to direct a water jet on the surface of the Pyrex frames. The frames were directly dropped afterwards into three successive isopropyl alcohol baths and dried with a canned air duster. All of this was done without any contact to the faces of the frames.

2.2.2.2 Thermal bonding

The different pieces were then stacked in the proper order into a stainless steel alignment frame and sandwiched between 2 silicon wafer pieces sprayed with boron nitride. The wafer pieces were obtained by spraying and drying boron nitride (Boron nitride aerosol Lubricoat®, Zyp Coatings, Inc, Oak Ridge, TN) on a polished silicon wafer being rotated at 600 rpm to obtain an even layer. The wafer was subsequently cut into pieces. A weight was added on top of the assembly. The total weight added on top of the Pyrex frames was 4 g. The alignment frame was designed to keep the Pyrex® frames aligned while the weights were added. The bonding was performed in a

Neytech™ 85P furnace (Neytech, Bloomfield, CT) at a temperature of 650°C and the bonding time was 6 hours.

2.2.3 Results

Figure 2.5(a) shows a bonded Pyrex® assembly consisting of 1 type A frame on top, followed by 2 type B frames and a back plate. The assembly is completely bonded, such that a hermetic bond completely surrounds the macroreservoirs and channels. Figure 2.5(b) shows the interface between two of the bonded plates. Trapped particles are visible, and are surrounded by interference fringes, denoting the unbonded space around the particle. Although several such particles are trapped within interfaces between frames, none threaten the hermeticity of this package.

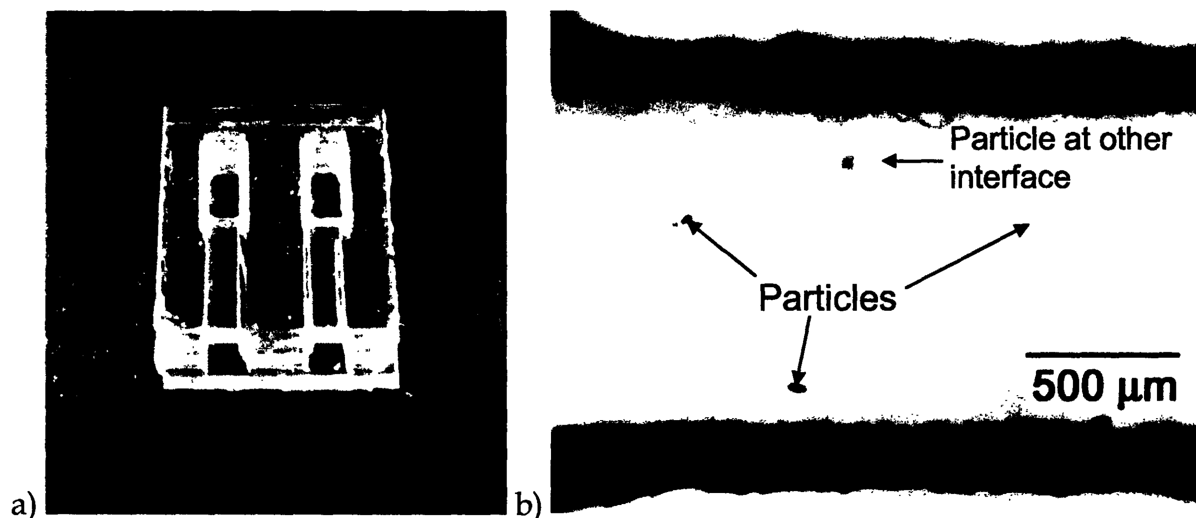

Figure 2.5: a) Thermally bonded Pyrex® assembly. The dimensions of the assembly are 5.5 mm (W) x 7.5 mm (L) x 2 mm (H). The access channels are clearly visible from the front. b) Interface between the macroreservoirs of (a). Particles surrounded by interference fringes indicate unbonded areas. They are scattered across the whole interface, but none of these particles are threatening the immediate hermeticity of the macroreservoirs.

2.2.4 Discussion

Figure 2.4(b) shows the reason why the bonding conditions are markedly increased from the mentioned 600°C and 30 minutes needed to bond 2 clean Pyrex® 7740 wafers. The particles that are still present after cleaning the Pyrex frames prevent intimate contact between the frames, although their number is cut down by cleaning. This means that more plastic flow is needed for the surfaces to come into contact and bond, hence the higher temperature, longer time and added compression load.

It is also to be noted that sometimes, particles are trapped in such a location that hermeticity is not achieved and leakage paths in the interface would allow drug to escape, if the assembly were to be used. The possibility also exists for previously harmless unbonded areas to grow and create leakage paths as a result of stresses, shocks or other external forces, if they are close to an edge, although this has not been verified.

The use of boron nitride sprayed silicon wafer pieces stemmed from the elevated conditions undergone while bonding. The bonding conditions were such that the Pyrex frames would partly bond to the substrate in contact with the assembly. Substrates that were experimented with included:

- polished aluminum oxide
- silicon nitride thin film on polished silicon wafer
- platinum thin film deposited on above substrate

The drawback of using sprayed boron nitride is that after bonding, the surfaces in contact with the boron nitride flowed and roughened, due to the topography of the boron nitride powder film in contact with the Pyrex. This roughness is deleterious to the anodic bonding process that is supposed to take place afterwards. That is why in the following chapter, the formed assembly is not bonded to a silicon chip, but rather, a single type A frame will be used.

The origin of the particles trapped at the interfaces is not known, but it could be as simple as the fact that the cleaning work was not done in a cleanroom, and particles in the air came in contact with the frames while stacking them. Contact also happens between the alignment stainless steel frame and the Pyrex® plates during stacking. The alignment frame is cleaned in the same manner as the Pyrex® frames, but it is again possible for particles in the air to come in contact with it.

The obvious but not easiest solution to this problem is to manage to get rid of all particles at the surface of Pyrex® frames to be bonded. This should be done in a cleanroom, since any cleaning will be ineffective if particles come in contact with the Pyrex® frames after cleaning. An alternative to the cleanroom could be a laminar flow hood. This hood is designed such that a downward laminar flow of air is set up inside. This prevents foreign particles in the air from reaching inside the hood and contaminating biological samples.

The bonding conditions would then be lowered, and there would be no need for a weight on the frames. Only one surface (that of the back plate) would need to be in

contact with a substrate. That would leave the prospective surface for anodic bonding free from any contact, and free from excessive plastic flow.

Using wafer-level bonding instead of chip-level bonding may also improve this process. The difference in bonding wafers instead of chips is that if a particle is trapped between two wafers, the weight of the wafer around it may be enough to force the glass at a distance around it to flow down and bond anyway. A Pyrex® frame does not have that advantage, because of its small size. It is not a perfect scheme, as unbonded areas would still be present, but regions that are bonded would not have had contact with any other surface, and would keep their low roughness. This depends of course on the density of trapped particles, which must be low enough for this to happen. A high density of particles would just distribute the weight of the wafer between the particles, and no bonding would occur. Performing wafer-level bonding would also require changing the fabrication scheme of the frames, however, as channels for type B frames can at present only be machined in finished type A frames.

Another solution to the problem is not to change the cleaning and bonding process, but recondition the surface of the Pyrex® assembly that is to be anodically bonded. Polishing the surface back to acceptable roughness may be achieved using chemical mechanical polishing (CMP). This technique uses chemical means in addition to conventional mechanical polishing, and can polish surfaces to very low roughness. It is the technique used in polishing wafers. It is however mostly done on a wafer level. Chip-level CMP is possible, but fixtures for it are not as widespread as for wafers. Future investigation should determine the feasibility of this option. This would again

not solve the problem of unbonded areas at interfaces, but may give a temporary solution while other options are pursued.

CHAPTER 3: ANODIC BONDING OF PYREX® TO SILICON CHIP

3.1 Introduction

Anodic bonding is a technique gaining in popularity in the MEMS processing field, because of its ability to bond glass to silicon or metals and create hermetic enclosures at relatively low temperatures, in ambient atmosphere or vacuum[27, 28, 43-58]. It is largely used in packaging of MEMS in fields such as sensors[44, 46, 50, 51], microfluidic applications[27, 28, 44, 46, 47], and optical MEMS[56, 57]. It is even used to bond glass to glass by using an intermediate metallic thin film[46, 54, 55]. Anodic bonding was chosen in this work as the only mechanism that would allow hermetic packaging of our drug delivery device without compromising the integrity of its membranes with high process temperatures[17].

3.2 Anodic bonding mechanism

The premise of anodic bonding is the joining of two dissimilar materials, a glass and a metal or semiconductor. Pyrex® 7740 is a good match for silicon because of their similar coefficient of thermal expansion (3.25×10^{-6} °C^{-1} for the former and 2.6×10^{-6} °C^{-1} for the latter). It is a borosilicate glass with the following approximate composition: SiO_2 (80.6%), B_2O_3 (13%), Na_2O (4%), Al_2O_3 (2.3%), K_2O (0.1%). The sodium ions from Na_2O are central to the anodic bonding process.

The generally accepted model for anodic bonding of Pyrex® 7740 to silicon is represented in Figure 3.1[43, 45]. It shows that when a large negative voltage (500-3000 V) is applied to the Pyrex® in contact with silicon, and at a sufficiently high temperature (250-400°C) for ionic conduction to occur, sodium ions diffuse away from the silicon-Pyrex® interface under the influence of the electric field. The cations reaching the cathode form either sodium metal or sodium-reduced glass constituents, according to the reaction:

$$Na^+ + e^- \rightarrow Na \quad (1)$$

The Pyrex® region next to the silicon is soon depleted of its mobile sodium ions[59, 60], and forms a depletion layer with excess negative charge at its edge in the glass, and excess positive charge to counter it in the silicon. This happens because the oxygen anions cannot diffuse nearly as fast as the sodium cations. The formation of this depletion layer has two consequences: first, it creates an electrostatic attraction between the silicon and glass, bringing them into intimate contact; and secondly, it becomes the region where most of the voltage drop occurs. This results in a very high electric field across the depletion layer, which is typically a few micrometers wide. This electric field is high enough to force motion of both cations (other than sodium) and anions. Oxygen anions are thus slowly transported across the depletion layer. The bond between silicon and the glass is formed when these oxygen anions diffuse into and oxidize silicon according to the reaction:

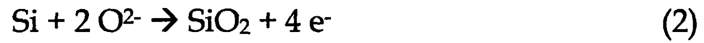

$$Si + 2\,O^{2-} \rightarrow SiO_2 + 4\,e^- \qquad (2)$$

The resulting silicon dioxide forms the bridge between the two materials, and a hermetic bond is formed[59].

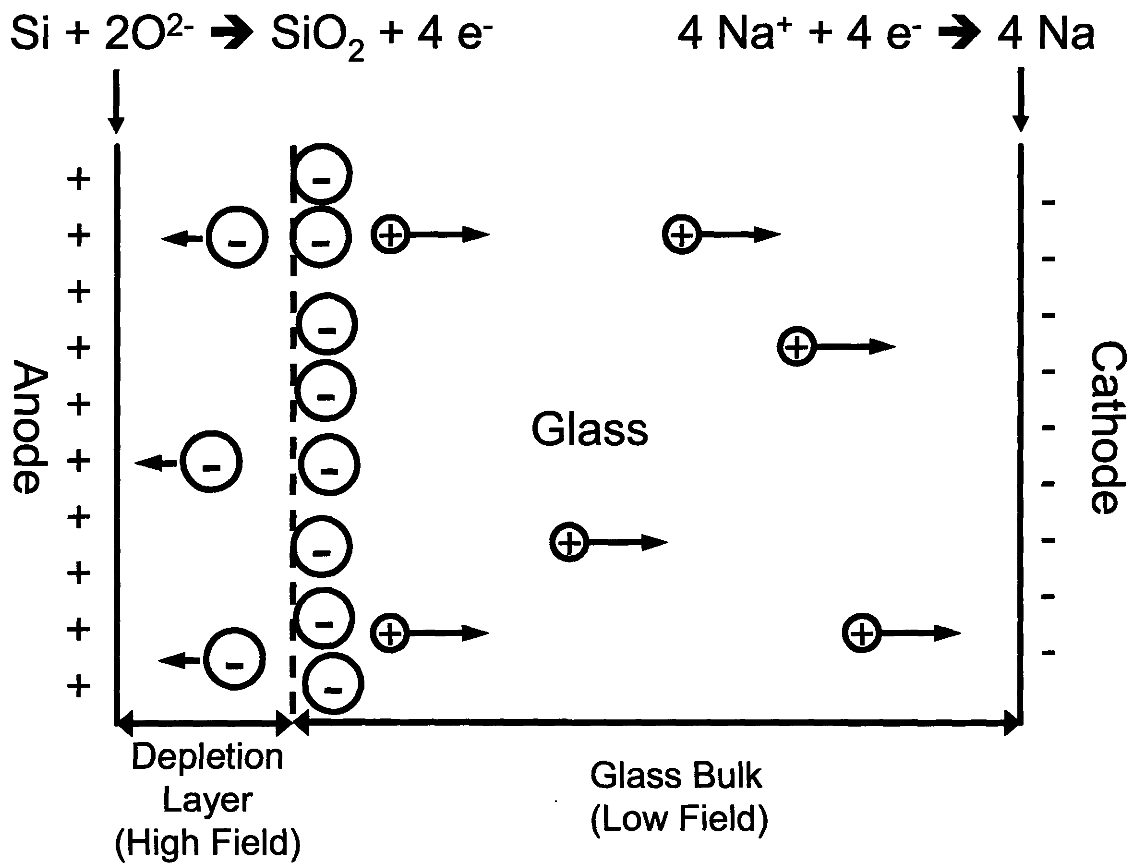

Figure 3.1: Schematic of anodic bonding mechanism of Pyrex® 7740 and silicon. Reproduced from reference [45].

3.3 Experimental procedure

3.3.1 Fixture

The bonding between the back face of the silicon chip and the Pyrex® assembly was done in a custom-built fixture. The front of the chip is protected by a dielectric layer, and thus cannot be electrically contacted from a metallic base. The sides of the chip are the only other place where electrical contacts can be made. Figure 3.2(a) shows the fixture with a chip inserted. The fixture is made of aluminum, and the chip is contacted by two razor blades (Single-edged No.9, VWR Scientific, Media, PA) on its sides. The razor blades are ~ 200 μm thick, making them ideal to contact the chip (320-μm thick) without preventing the larger Pyrex® frames from contacting the chip. Two screws are used to fix each blade. A straight aluminum oxide edge is present to facilitate alignment of the chip with the Pyrex frames.

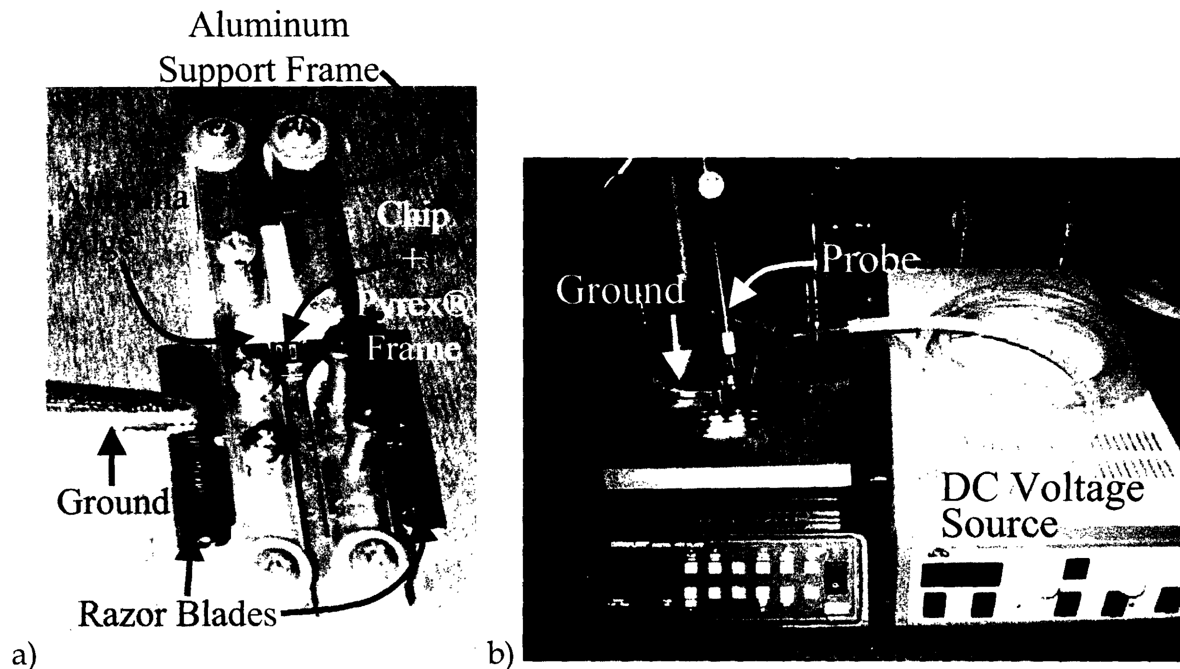

Figure 3.2: a) Picture of the anodic bonding fixture. An aluminum frame supports screws that hold razor blades (for contact) and an alumina edge (for alignment) in position. The Pyrex® frame with its two macroreservoirs covering the chip is visible in the middle of the fixture. The fixture is grounded through one of the razor blades. b) Picture of the experimental setup used for anodic bonding process. The fixture, with the chip and Pyrex® frame, is set on a hot plate at 300°C and grounded. A probe connected to the DC voltage source is lowered onto the Pyrex frame. The voltage (-1000 V) is applied after the fixture and chip have heated up to temperature.

3.3.2 Anodic bonding procedure

Figure 3.2(b) shows the experimental setup as described hereafter. The chip and a type A Pyrex® frame were cleaned with acetone, followed by methanol and isopropyl alcohol. The chip was first set into the fixture and the razor blades brought into contact and fixed. The Pyrex® frame was then set on the chip and visually aligned. The fixture was set on a hot plate at 300°C and electrically grounded, then left to equilibrate to the set temperature for 10 minutes. A probe was lowered onto the Pyrex frames to apply a

DC negative potential of -1000 V using a high voltage source (Model 677B, Trek, Inc, Medina, NY).

4 points were contacted in succession by the probe as shown on Figure 3.3. This was needed because of the geometry of the Pyrex frame, which has 2 large macroreservoirs that reduce the electric field beyond them. Total bonding time was ~25 minutes. Currents were less than 10 uA and not detected by the power source, because of the small amount of surface being contacted (~15 mm^2). The bonded devices were soaked in DI water overnight to dissolve the sodium deposited at the surface of the Pyrex® frame.

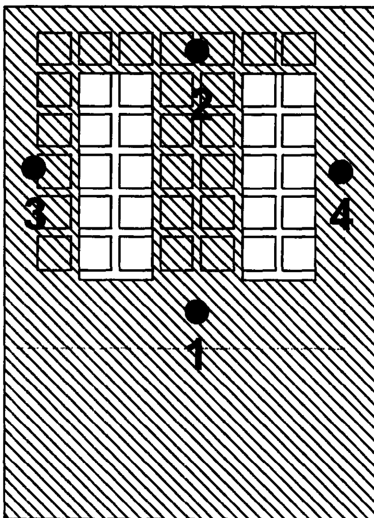

Figure 3.3: Locations of successive probe placement for anodic bonding. The probe was left 7.5 minutes at points 1 and 2, and 5 minutes at points 3 and 4 in order to accelerate the bonding.

3.4 Results

Figure 3.4 shows an optical micrograph of the bonded interface around a macroreservoir. The dark color of the silicon streets between the microreservoirs

indicates that bonding occurred. The picture also shows good alignment of the macroreservoir to the chip. Some light-colored spots indicate unbonded areas, but none of them are of immediate consequence for the hermeticity of the macroreservoir.

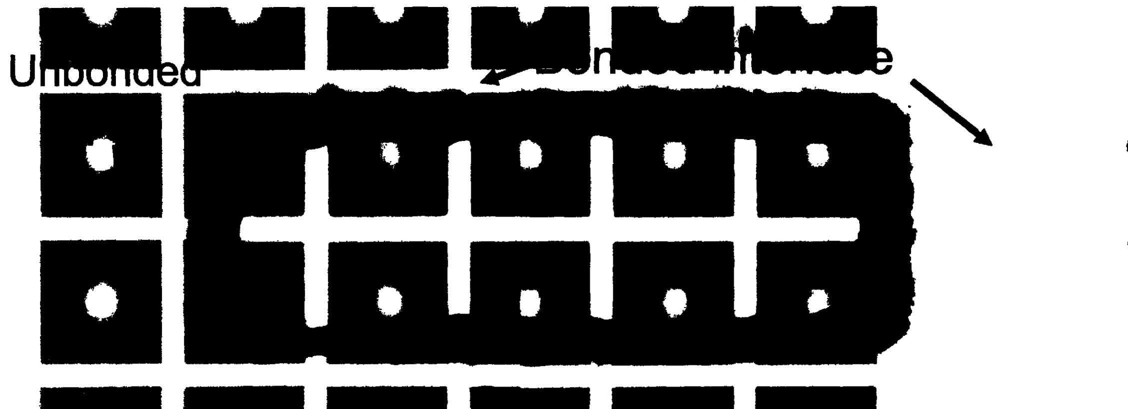

Figure 3.4: Optical micrograph of hermetically bonded interface of a type A Pyrex® frame and silicon chip. The dark color of the silicon denotes bonded material, and the light spots denote unbonded spots due to trapped particles. The changing color of the bonded interface between left and right is an artifact of the microscopy.

3.5 Discussion

Figure 3.4 shows that the process was successful, and that visual alignment of the frame to the chip was sufficient to obtain good alignment. In the future case where a whole Pyrex® assembly will be bonded to the chip, use of a stereomicroscope may be needed in order to see through all the layers and avoid reflections from the back plate.

There is also some concern pertaining to the existence of the unbonded spots. It is the potential presence of those spots at the outer edge of the interface between Pyrex® and the silicon chip. Such a case has been observed while performing anodic bonding. These

spots can act as initial cracks for catastrophic failure of the interface if they were to undergo severe shocks (like a drop onto the floor), since both materials are brittle. Care must therefore be taken to avoid cases where unbonded spots are at the edge of the chip, even if the seal to the macroreservoirs itself is not initially compromised, as that could be changed in an instant with a severe shock.

This problem comes back again to the issue of cleanliness. The anodic bonding work was done in a Class 1000 cleanroom, but it is obvious that particles were still able to be trapped at the interface between silicon and Pyrex®. This problem is however less serious than that encountered in thermal bonding of Pyrex®, because of the electrostatic attraction inherent to the process. This work may have to be done in a laminar flow hood in the future, depending on the quality of the particle count in such a hood.

The use of sprayed boron nitride powder in bonding the Pyrex® frames together resulted in a surface roughness not suitable for anodic bonding, as discussed in the previous chapter. It was not possible to directly hermetically bond these assemblies to a chip, because of dimples in the glass surface left by the boron nitride powder layer. A decision was made to bond only one type A frame to the back of the chip, in the interest of obtaining a usable chip package in a short time. The following chapter describes the final step in the completion of the package.

CHAPTER 4: VALIDATION OF THE PACKAGE

4.1 Package completion

A silicon chip anodically bonded to a type A frame was glued to a Pyrex® assembly comprised of 2 type B frames and a back plate, with a UV-cured epoxy (1-20542 cationic epoxy, Dymax Corp, Torrington, CT). A thin layer of epoxy was applied to the Pyrex® surface using the principle of offset printing.

A silicone mold is patterned with shallow parallel ridges. The epoxy is applied to the mold and excess epoxy is wiped off using a rubber squeegee, leaving epoxy only between the ridges. This ensures that the amount of epoxy delivered is constant. The Pyrex® assembly is pressed onto the surface of the mold to transfer the epoxy to the assembly surface. The assembly is then pressed onto the anodically bonded chip-Pyrex® assembly and the epoxy is cured by exposure to UV light, without applying additional compressive loads. UV exposure time is 20 seconds with the spot curing system ADAC Systems™ CURE SPOT™ 50 (Dymax Corp). Figure 4.1 shows the completed packaged device next to the previous stainless steel package.

The size of this new package is 5.5 mm x 7.5 mm x 2.5 mm, compared to 11 mm x 11 mm x 2.5 mm. Its maximum nominal capacity is 8.9 µL (0.5 µL for 20 microreservoirs, and 3 plates with 1.4 µL macroreservoirs), compared to 0.9 µL, a tenfold increase. The capacity can be further increased by adding more type A frames to the Pyrex® assembly.

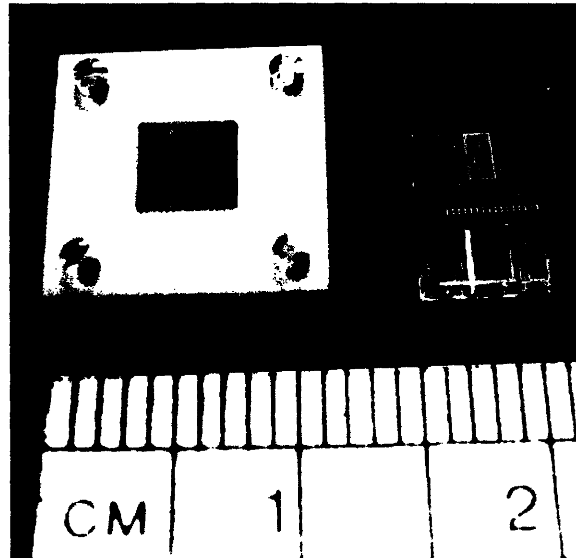

Figure 4.1: Stainless steel package and Pyrex package for the drug delivery MEMS. The size advantage of the latter is obvious.

4.2 Experimental validation

The following experimental validation was performed by Yawen Li with the newly developed package and publication of the following data is done with her permission. Further experimental details for all experiments can be found in reference [17].

4.2.1 Filling of devices

Injection of drugs into the macroreservoirs was performed under a stereomicroscope using a micropump system consisting of a UMP-1 Ultra Micro Pump with Micro-1 controller and a Kite-R micromanipulator with a TB-1 tilting base (all from World Precision Instruments, Sarasota, FL). Each solution was injected from a 10 μL syringe fitted with a 32-gauge needle (Hamilton Company, Reno, NV). The access channel

openings were then covered with Ideal 9144 Masking Tape (American Biltrite, Inc, Lowell, MA) and the tape was held in place with UV-cured epoxy.

4.2.2 Hermeticity

The hermeticity of the fabricated package was tested with the following procedure. A Pyrex® packaged chip was injected with an 80:20 volume ratio solution of BCNU (Bristol-Myers Squibb Co., Evansville, IN) and polyethylene glycol (PEG, MW 200, Carbowax™, Dow Chemical Company, Midland, MI), including some ^{14}C radiolabeled BCNU (Moravek Biochemicals, Brea, CA) with a total radioactivity of 0.25 µCi. Each macroreservoir received 1 µL of solution. The device was sealed and submerged in deionized water at room temperature. 1 mL aliquots were collected and replaced at each data point, and radioactivity was measured by mixing each sample with 5 mL of ScintiSafe fluid (Fisher Scientific, Atlanta, GA) and counting radioactivity in a Packard Tri-Carb liquid scintillation analyzer (Model 2200CA, Perkin-Elmer Life Sciences, Downers Grove, IL). Figure 4.2 shows the results of the experiment, along with results from the leakage test shown in Figure 1.5. The package showed no leakage at all until after the 12th day, where it increased dramatically.

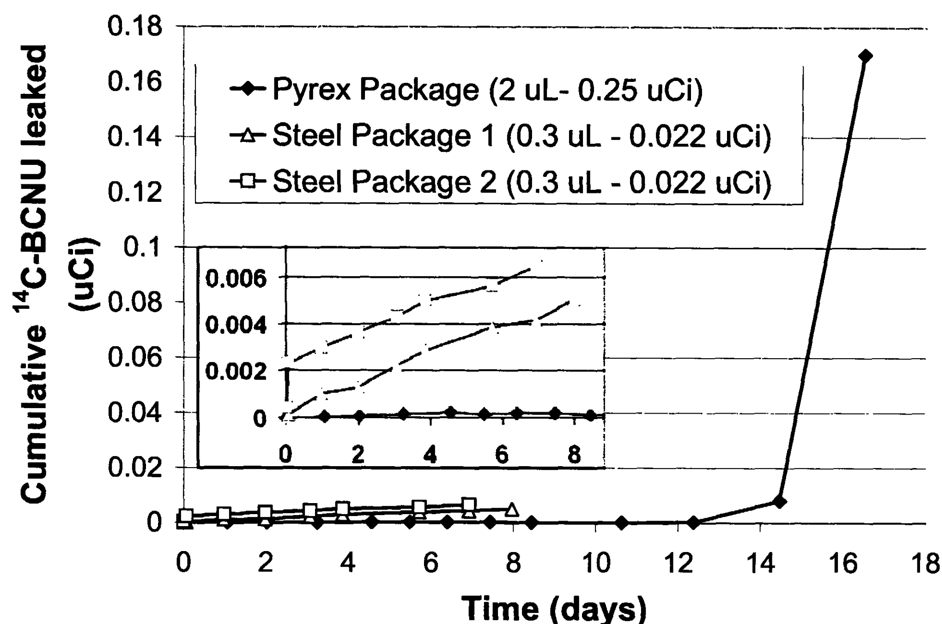

Figure 4.2: Leakage test of a Pyrex® packaged device, compared to the stainless steel packaged devices from Figure 1.5. The Pyrex® packaged device was filled with a 2 μL mixed solution of BCNU and PEG with 80:20 volume ratio and a total radioactivity of 0.25 μCi ^{14}C-BCNU. The stainless steel packaged devices were filled with ^{14}C-BCNU and 22 nL PEG per microreservoir, for a total volume of 0.3 μL and a total radioactivity of 0.022 μCi per chip. The scale for the y-axis is not relative to the initial loading of drug, but is the actual detected radioactivity leaked out of the chips. The radioactivity count for the Pyrex® packaged device is practically zero until day 12 (~300 hours). Data courtesy of Yawen Li.

4.2.3 *In vitro* release

Figure 4.3 shows an *in vitro* release experiment where mixtures of BCNU and PEG in different volume ratios were injected into Pyrex® packaged chips. The amount of BCNU injected was kept the same, except for the device with 80% PEG, which had a little less BCNU. The macroreservoirs were sealed as described in Section 4.2.1. Figure 4.3 shows an average release of 90% of the initial loading, after 2 activations releasing half of the loading each.

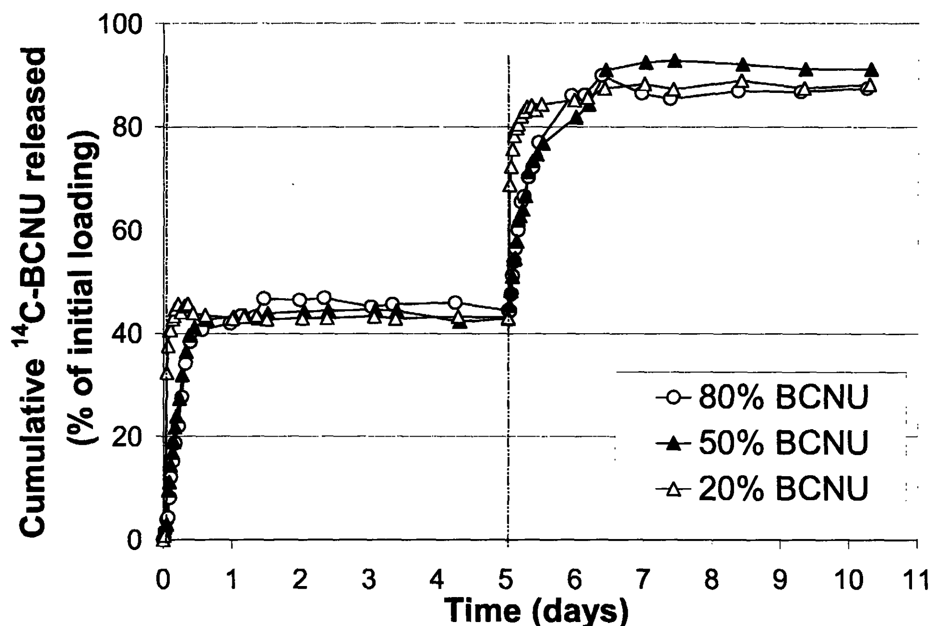

Figure 4.3: Cumulative percentages of ^{14}C-BCNU released from three Pyrex® packaged devices. Each activation (denoted by the dashed line) corresponds to the opening of 10 microreservoirs with half of the initial loading. Each device was filled with a mixed solution of ^{14}C-BCNU/BCNU/PEG with different BCNU/PEG volume ratio. The BCNU loading was 1.2 mg in the devices with 50% and 80% BCNU, and 0.96 mg in the device with 20% BCNU. Test performed at room temperature in PBS. Reprinted with permission from reference [17].

4.3 Discussion

The hermeticity test of the package shows that the package has much better hermeticity to BCNU for up to 12 days, compared to the stainless steel package, which leaked from the beginning. Figure 4.4 shows an interface between two Pyrex® plates bonded with UV-cured epoxy that has been attacked by BCNU. It suggests that the dramatic leakage seen after 12 days is due to the failure of the epoxy bonding the Pyrex® assembly to the anodically bonded chip assembly. The epoxy could not resist prolonged contact with

the BCNU solution and failed. It can be inferred from this result that internal hermeticity of the chip was also compromised.

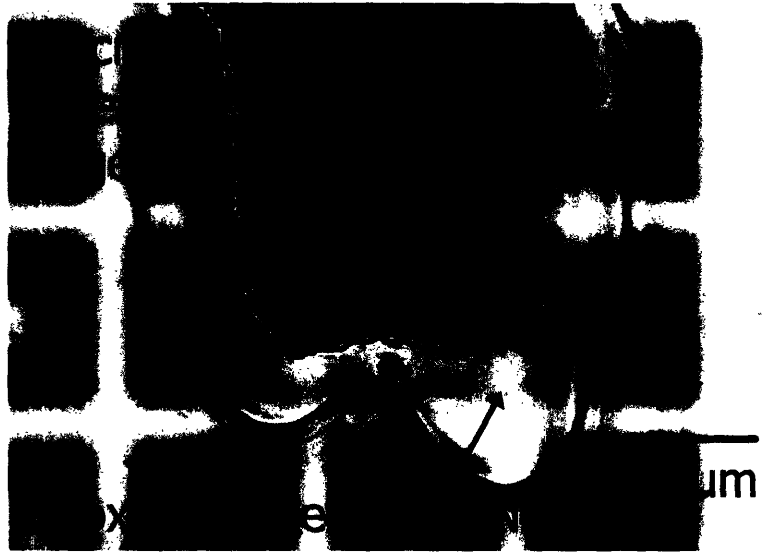

Figure 4.4: Optical micrograph of the interface of a type A Pyrex® frame and a back plate bonded with UV-cured epoxy. BCNU was injected into this macroreservoir and was seen attacking the epoxy after a few days. The black line outlines the edge of the macroreservoir for clarity. Picture courtesy of Malinda Tupper.

This is an argument for the continuing development of the package. This problem stems from the inability to bond the thermally bonded Pyrex assembly to the silicon chip, as mentioned previously. The correcting steps discussed in Section 2.2.4 will hopefully lead to a permanent solution.

The hermeticity experiment and *in vitro* release of BCNU both demonstrate the increased capacity of the new package, as more than 0.9 μL of solution was contained in each chip that was tested. The *in vitro* release also saw the release of 90% of the initial loading, a marked improvement compared to the 40% that were released by the

stainless steel package. It is postulated that the remaining 10% were trapped where the UV-cured epoxy was attacked between the two Pyrex® frames bonded with it, since the experiment lasted 10 days. Removing the use of UV-cured epoxy to bond Pyrex® plates should allow the remaining drug to be released.

Another advantage of the new package mentioned at the beginning of this chapter, which was not necessarily envisioned when designing it, is its smaller size compared to the stainless steel package. The volume of this package is 3 times less than the volume of the previous package (~100 mm^3 vs. 300 mm^3), making it possible to implant more than one device to treat a tumor.

CHAPTER 5: CONCLUSION AND FUTURE WORK

A new package was designed and fabricated from Pyrex® 7740 with the purpose of increasing the load capacity of a MEMS drug delivery device, achieving complete release of the loaded drug, as well as improving its internal and environmental hermeticity. The successful fabrication of the package described in this thesis signals a milestone in the improvement of our chip package. The goal of increasing chip capacity was satisfactorily reached and the size of the new package was reduced by a factor of three. The loaded drug was also almost completely released. Internal and environmental hermeticity were excellent for short-term situations, but the package failed at longer times, as fabrication of the package using only thermal bonding and anodic bonding was not achieved. Future work on this subject will focus on improving the fabrication of the Pyrex® assembly, by perfectly cleaning the Pyrex® frames to be bonded; implementing wafer-level Pyrex® thermal bonding; or reconditioning the Pyrex® surface to be anodically bonded, post-thermal bonding.

REFERENCES

1. Brem, H., Piantadosi, S. *et al*, *Placebo-controlled Trial of Safety and Efficacy of Intraoperative Controlled Delivery by Biodegradable Polymers of Chemotherapy for Recurrent Gliomas.* Lancet, **345**(8956): p. 1008-1012 (1995)
2. Brem, H. and Langer, R., *Polymer Based Drug Delivery to the Brain.* Sci Am Sci Med, **75**: p. 922-929 (1996)
3. Gravesen, P., Branebjerg, D., and Jensen, O.S., *Microfluidics: A Review.* Journal of Micromechanics and Microengineering, **3**: p. 168 - 182 (1993)
4. Kost, J. and Langer, R., *Responsive Polymeric Delivery Systems.* Advanced Drug Delivery Reviews, **6**: p. 19 - 50 (1991)
5. Kwon, I.C., Bae, Y.H., and Kim, S.W., *Electrically erodible polymer gel for controlled release of drugs.* Nature, **354**: p. 291-293 (1991)
6. Mathiowitz, E. and Cohen, M.D., *Polyamide Microcapsules for Controlled Release. V. Photochemical Release.* Journal of Membrane Science, **40**(1): p. 67 - 86 (1989)
7. Rhines, L.D., Sampath, P. *et al*, *Local immunotherapy with interleukin-2 delivered from biodegradable polymer microspheres combined with interstitial chemotherapy: A novel treatment for experimental malignant glioma.* Neurosurgery, **52**(4): p. 872-878 (2003)
8. Sampath, P., Hanes, J. *et al*, *Paracrine immunotherapy with interleukin-2 and local chemotherapy is synergistic in the treatment of experimental brain tumors.* Cancer Research, **59**: p. 2107-2114 (1999)
9. Santini, J.T., Cima, M.J., and Langer, R., *A controlled-release microchip.* Nature, **397**: p. 335-338 (1999)
10. Santini, J.T., Richards, A.C. *et al*, *Microchips as controlled drug-delivery devices.* Angew Chem Int Ed, **39**: p. 2396-2407 (2000)
11. Tamargo, R.J., Myseros, J.S. *et al*, *Interstitial Chemotherapy of the 9L Gliosarcoma: Controlled Release Polymers for Drug Delivery in the Brain.* Cancer Research, **53**(2): p. 329-333 (1993)
12. Thielicke, E. and Obermeier, E., *Microactuators and their technologies.* Mechatronics, **10**: p. 431-455 (2000)
13. Hanes, J., Sills, A. *et al*, *Controlled local delivery of interleukin-2 by biodegradable polymers protects animals from experimental brain tumors and liver tumors.* Pharmaceutical Research, **18**(7): p. 899-906 (2001)
14. Thompson, R.C., Pardoll, D. *et al*, *Systemic and paracrine cytokine therapy using transduced tumor cells are synergistic in treating intracranial tumors.* Journal of Immunotherapy, **19**(6): p. 405-413 (1996)
15. Farone and Cox, *BCNU/IL-2 chemoimmunotherapy of murine L1210 leukemia.* Cancer Immunology and Immunotherapy, **34**(4): p. 279-281 (1992)
16. Li, Y., Shawgo, R.S. *et al*, *In vivo release from a drug delivery MEMS device.* Journal of Controlled Release, **100**(2): p. 211-219 (2004)

17. Li, Y., *Ph.D. Thesis. Mechanical characterization and in vivo operation of an implantable drug delivery MEMS device*. Massachusetts Institute of Technology: Cambridge, MA (2005)
18. Shawgo, R.S., Voskerician, G. *et al, Repeated in vivo electrochemical activation and the biological effects of microelectromechanical systems drug delivery device.* Journal of Biomedical Materials Research Part A, **71A**(4): p. 559-568 (2004)
19. Shawgo, R.S., *Ph.D. Thesis. In vivo activation and biocompatibility of a MEMS microreservoir drug delivery device.* Massachusetts Institute of Technology: Cambridge, MA (2004)
20. Voskerician, G., Shivea, M.S. *et al, Biocompatibility and Biofouling of MEMS Drug Delivery Devices.* Biomaterials, **24**(11): p. 1959 - 1967 (2003)
21. Voskerician, G., Shawgo, R.S. *et al, In Vivo Inflammatory and Wound Healing Effects of Gold Electrode Voltammetry for MEMS micro-reservoir drug delivery device.* IEEE Transactions on Biomedical Engineering, **51**(4): p. 627-635 (2004)
22. Shawgo, R.S., Sheppard Jr., N.F. *et al, US Patent: Methods and Devices for Sealing Microchip Reservoir Devices*. Massachusetts Institute of Technology: United States of America (2001)
23. Thoe, T.B., Aspinwall, D.K., and Wise, M.L.H., *Review on Ultrasonic Machining.* International Journal of Machine Tools and Manufacture, **38**(4): p. 239-255 (1998)
24. Li, X.G., Abe, T. *et al, Fabrication of high-density electrical feed-throughs by deep-reactive-ion etching of Pyrex glass.* Journal of Microelectromechanical Systems, **11**(6): p. 625-630 (2002)
25. Li, L., Abe, T., and Esashi, M., *Smooth surface glass etching by deep reactive ion etching with SF6 and Xe gases.* Journal of Vacuum Science & Technology B, **21**(6): p. 2545-2549 (2003)
26. Li, X., Abe, T., and Esashi, M., *Deep reactive ion etching of Pyrex glass using SF[6] plasma.* Sensors and Actuators A: Physical, **87**: p. 139-145 (2001)
27. Bu, M., Melvin, T. *et al, A new masking technology for deep glass etching and its microfluidic application.* Sensors and Actuators A: Physical, **115**(2-3): p. 476-482 (2004)
28. Verpoorte, E. and De Rooij, N.F., *Microfluidics meets MEMS.* Proceedings of the IEEE, **91**(6): p. 930-953 (2003)
29. Hulsenberg, D., *Glasses for Microsystems Technology.* Microelectronics Journal, **28**: p. 419-432 (1997)
30. Pawlowski, A.G., Belloy, E. *et al, Powder blasting patterning technology for microfabrication of complex suspended structures in glass.* Microelectronic Engineering, **67-8**: p. 557-565 (2003)
31. Schlautmann, S., Wensink, H. *et al, Powder-Blasting Technology as an Alternative Tool for Microfabrication of Capillary Electrophoresis Chips with Integrated Conductivity Sensors.* Journal of Micromechanics and Microengineering, **11**: p. 386-389 (2001)
32. Solignac, D., Sayah, A. *et al, Powder blasting for the realisation of microchips for bio-analytic applications.* Sensors and Actuators A: Physical, **92**: p. 388-393 (2001)

33. Wensink, H., Berenschot, J.W. *et al. High Resolution Powder Blast Micromachining.* in *The 13th Annual International Conference on Micro Electro Mechanical Systems. MEMS 2000.* 2000: IEEE.
34. Fujii, H., Tanabe, H. *et al, A sandblasting process for fabrication of color PDP phosphor screens.* SID 92 Digest: p. 728-731 (1992)
35. Busio, M. and Steigelmann, O., *New frit glasses for displays.* Glass Science and Technology-Glastechnische Berichte, **73**(10): p. 319-325 (2000)
36. Kim, Y.H., Lee, H.W. *et al, Formation of barrier ribs for plasma display panels via powder-blasting process: Part II, effects of powder-blasting angle.* Journal of the American Ceramic Society, **87**(3): p. 348-351 (2004)
37. Kim, Y.H., Lee, H.W. *et al, Formation of barrier ribs for plasma display panels via a powder-blasting process: Part I, effects of binder content and baking treatment.* Journal of the American Ceramic Society, **87**(3): p. 342-347 (2004)
38. Tilly, G.P. and Sage, W., *The Interaction of Particle and Material Behaviour in Erosion Processes.* Wear, **16**: p. 447-465 (1970)
39. Slikkerveer, P.J., Bouten, P.C.P. *et al, Erosion and damage by sharp particles.* Wear, **217**: p. 237-250 (1998)
40. Wensink, H., Jansen, H.V. *et al, Mask materials for powder blasting.* Journal of Micromechanics and Microengineering, **10**(2): p. 175-180 (2000)
41. Corning, *Pyrex® 7740 Data Sheet:* http://www.corning.com/lightingmaterials/images/wafersheet.pdf (1999)
42. Li, Y., *Personnal Communication, 21 April 2004,* (2004)
43. Albaugh, K.B., Cade, P.E., and Rasmussen, D.H. *Mechanisms of Anodic Bonding of Silicon to Pyrex Glass.* in *Solid-State Sensor and Actuator Workshop.* 1988: IEEE.
44. Brennan, D., O'Brien, P. *et al, Development and test of an integrated microsystem for HPLC separation and detection using refractive index measurements.* Sensors and Actuators B-Chemical, **103**(1-2): p. 184-189 (2004)
45. Albaugh, K.B. and Rasmussen, D.H., *Rate Processes during Anodic Bonding.* Journal of the American Ceramic Society, **75**(10): p. 2644-48 (1992)
46. Kameoka, J. and Craighead, H.G., *Nanofabricated refractive index sensor based on photon tunneling in nanofluidic channel.* Sensors and Actuators B-Chemical, **77**(3): p. 632-637 (2001)
47. Lee, D.S., Yoon, H.C., and Ko, J.S., *Fabrication and characterization of a bidirectional valveless peristaltic micropump and its application to a flow-type immunoanalysis.* Sensors and Actuators B-Chemical, **103**(1-2): p. 409-415 (2004)
48. Llobera, A., Plaza, J.A. *et al, Technological aspects on the fabrication of silicon-based optical accelerometer with ARROW structures.* Sensors and Actuators A: Physical, **110**(1-3): p. 395-400 (2004)
49. Nimkar, N.D., Bhavnani, S.H. *et al, Development of an anodically-bonded test surface to obtain fundamental liquid immersion thermal management data for electronic devices.* Sensors and Actuators A: Physical, **113**(2): p. 212-217 (2004)
50. Plaza, J.A., Lopez-Bosque, M.J. *et al, A glass/silicon technology for low-power robust gas sensors.* IEEE Sensors Journal, **4**(2): p. 195-206 (2004)

51. Rogers, T. and Kowal, J., *Selection of Glass, Anodic Bonding Conditions and Material Compatibility for Silicon-Glass Capacitive Sensors.* Sensors and Actuators A: Physical, **46**(1-3): p. 113-120 (1995)
52. Schjolberg-Henriksen, K., Jensen, G.U. *et al*, *Anodic bonding for monolithically integrated MEMS.* Sensors and Actuators A: Physical, **114**(2-3): p. 332-339 (2004)
53. Lee, B., Seok, S., and Chun, K., *A study on wafer level vacuum packaging for MEMS devices.* Journal of Micromechanics and Microengineering, **13**(5): p. 663-669 (2003)
54. Kutchoukov, V.G., Laugere, F. *et al*, *Fabrication of nanofluidic devices using glass-to-glass anodic bonding.* Sensors and Actuators A: Physical, **114**(2-3): p. 521-527 (2004)
55. Wei, J., Nai, S.M.L. *et al*, *Glass-to-glass anodic bonding process and electrostatic force.* Thin Solid Films, **462-63**: p. 487-491 (2004)
56. Abeysinghe, D.C., Ranatunga, V. *et al*, *A novel technique for high-strength direct fiber-to-Si submount attachment using field-assisted anodic bonding for optoelectronics packaging.* IEEE Photonics Technology Letters, **16**(9): p. 2150-2152 (2004)
57. Muller, J., *MEMS on silicon for integrated optic metrology and communication systems.* Microsystem Technologies-Micro-and Nanosystems-Information Storage and Processing Systems, **9**(5): p. 308-315 (2003)
58. Briand, D., Weber, P., and De Rooij, N.F., *Bonding properties of metals anodically bonded to glass.* Sensors and Actuators A: Physical, **114**: p. 543-549 (2004)
59. Xing, Q.F., Yoshida, M., and Sasaki, G., *TEM study of the interface of anodic-bonded Si/glass.* Scripta Materialia, **47**(9): p. 577-582 (2002)
60. van Helvoort, A.T.J., Knowles, K.M., and Fernie, J.A., *Characterization of cation depletion in pyrex during electrostatic bonding.* Journal of the Electrochemical Society, **150**(10): p. G624-G629 (2003)